J. Microbiol. Biotechnol. (2019), 29(4), 577–586
https://doi.org/10.4014/jmb.1812.12064

jmb

Heteroexpression and Functional Characterization of Glucose 6-Phosphate Dehydrogenase from Industrial *Aspergillus oryzae*

Hongwei Guo, Jinyao Han, Jingjing Wu, and Hongwen Chen*

School of Chemical Engineering, Huaqiao University, Xiamen 361021, P.R. China

Received: December 30, 2018
Revised: January 25, 2019
Accepted: January 29, 2019

First published online
February 8, 2019

**Corresponding author*
Phone: +86-592-6162347;
E-mail: chenhw@hqu.edu.cn

Supplementary data for this paper are available on-line only at http://jmb.or.kr.

pISSN 1017-7825, eISSN 1738-8872

The engineered *Aspergillus oryzae* has a high NADPH demand for xylose utilization and overproduction of target metabolites. Glucose-6-phosphate dehydrogenase (G6PDH, E.C. 1.1.1.49) is one of two key enzymes in the oxidative part of the pentose phosphate pathway, and is also the main enzyme involved in NADPH regeneration. The open reading frame and cDNA of the putative *A. oryzae* G6PDH (AoG6PDH) were obtained, followed by heterogeneous expression in *Escherichia coli* and purification as a his6-tagged protein. The purified protein was characterized to be in possession of G6PDH activity with a molecular mass of 118.0 kDa. The enzyme displayed maximal activity at pH 7.5 and the optimal temperature was 50°C. This enzyme also had a half-life of 33.3 min at 40°C. Kinetics assay showed that AoG6PDH was strictly dependent on $NADP^+$ (K_m = 6.3 μM, k_{cat} = 1000.0 s^{-1}, k_{cat}/K_m =158.7 $s^{-1}\cdot\mu M^{-1}$) as cofactor. The K_m and k_{cat}/K_m values of glucose-6-phosphate were 109.7 $s^{-1}\cdot\mu M^{-1}$ and 9.1 $s^{-1}\cdot\mu M^{-1}$ respectively. Initial velocity and product inhibition analyses indicated the catalytic reaction followed a two-substrate, steady-state, ordered BiBi mechanism, where $NADP^+$ was the first substrate bound to the enzyme and NADPH was the second product released from the catalytic complex. The established kinetic model could be applied in further regulation of the pentose phosphate pathway and NADPH regeneration of *A. oryzae* to improve its xylose utilization and yields of valued metabolites.

Keywords: Pentose phosphate pathway, glucose-6-phosphate dehydrogenase, xylose, *Aspergillus oryzae*, ordered Bi-Bi mechanism

Introduction

Applying consolidated bioprocessing (CBP) technology is one of the most cost-effective routes for producing biofuels and chemicals, including ethanol, butanol and xylitol, directly from renewable biomass [1]. *Aspergillus oryzae*, as a Generally Recognized as Safe microbe, has been widely utilized in traditional food processing for centuries [2]. Known for its secretion of ligninolytic and hydrolytic enzymes [3], this filamentous fungus strain has been used to produce biodiesel, lipids and enzymes directly from lignocellulosic feed stocks [4–6]. The hydrolysates of the lignocellulose contain a mixture of glucose and xylose, [7] although the poor utilization of xylose remains the dominant hurdle to overcome with this organism [8].

In *A. oryzae*, the utilization of xylose is via three enzyme reactions involving xylose reductase, xylitol dehydrogenase and xylulokinase, to form xylulose 5-phophate, which enters the pentose phosphate pathway (PP pathway) (Fig. 1) [9]. Among these enzyme reactions, the metabolic flux of xylose metabolism has been tightly regulated by the activity of NADPH-dependent xylose reductase [10]. Metabolic strategies to enhance cofactor supply and regeneration have been extensively applied for improving xylose utilization and desired metabolite production in *E. coli*, *Candida tropicalis* and *Saccharomyces cerevisiae* [11–13]. Whereas, cofactor engineering strategies were seldom reported in *A. oryzae* for improving xylose utilization; even genes contributing to cofactor catabolism and biosynthesis were not well studied.

In many species, the main source of NADPH and its generation is the oxidative part of the PP pathway.

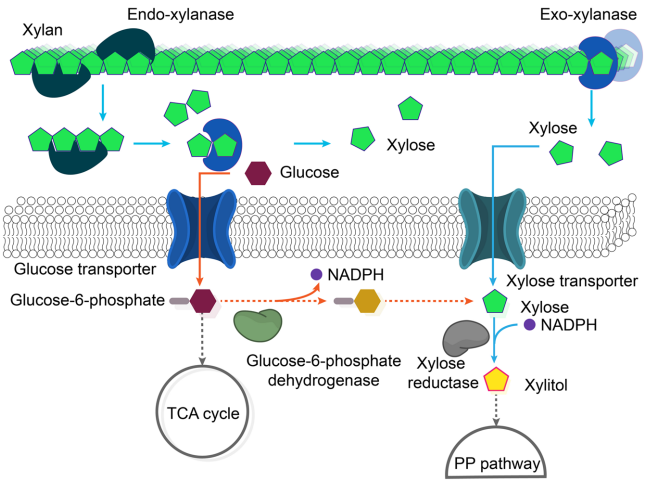

Fig. 1. Production of xylitol in *A. oryzae* from xylan.

Glucose-6-phosphate dehydrogenase (*gsd*, G6PDH, E.C. 1.1.1.49) is the first enzyme in the PP pathway and converts glucose-6-phosphate (G6P) to 6-phosphate-gluconolactone with concomitant generating of NADPH or NADH. In eukaryotic cells, the expression level of G6PDH is relatively constant [14, 15] and it was also reported that the catalysis of G6PDH was the rate-limiting catalytic step of the PP pathway [14, 16]. Accordingly, the potential for improving xylose utilization by regulation of G6PDH activity is high. However, in the genome database of *A. oryzae*, the open reading frame (ORF) of *gsd* is annotated as a tentative G6PDH. Gene verification and functional characterization of G6PDH from industrial *A. oryzae* (AoG6PDH) were also lacking.

The successful cloning and expression of the *gsd* and the characterization of the purified recombinant G6PDH from *A. oryzae* CICC2012 are only being reported here for the first time. The two-substrate, steady-state kinetic analysis, in addition to product and substrate inhibition studies, have also been established. This study provides essential clues into further regulation of the NADPH regeneration of *A. oryzae* to improve its production of the valued metabolites.

Materials and Methods

Strains and Culture Conditions

Glucose peptone (GP) medium containing 20 g/l glucose, 10 g/l peptone, 5 g/l KH_2PO_4, 1 g/l $NaNO_3$, 1 g/l $MgSO_4{\cdot}7H_2O$ was used for cultivating *A. oryzae* CICC2012 (China Industrial Microbiological Culture Collection Center) in a 250-ml shaker flask (150 rpm) for 3 days at 30°C, pH 6.0. LB medium supplemented with ampicillin (100 μg/ml) was used for cultivating *E. coli* strains at 37 °C. The *E. coli* DH5α was used for plasmid propagation and *E. coli* BL21 (DE3) was used for protein heterogeneous expression. Super Optimal broth with Catabolite repression (SOC) medium containing 20 g/l tryptone, 5 g/l yeast extract, 5 g/l NaCl, 2.5 mM KCl, 10 mM $MgCl_2$, 20 mM glucose was used to transform plasmid into competent cells at 37°C and pH 7.0, and this was followed by spreading in LB plates for 12 h at 37°C. And TB medium containing 12 g/l peptone, 24 g/l yeast extract, 2.3 g/l KH_2PO_4, 16.4 g/l K_2HPO_4, 5 g/l glycerol and isopropyl β-D-thiogalactoside (IPTG) was used for the induced expression of proteins.

Chemicals and Plasmids

Plasmid pUC19T-vector (pUCm-T), pET-28a(+), Taq DNA polymerase, RNase A, dNTP, DNA Gel Extraction Kit and EZ Column Plasmid Mini-Preps Kit were purchased from Sangon (China). Ligation reagents, restriction endonucleases and DNA marker were purchased from TaKaRa (China).

Obtaining of ORF and CDS of *gsd*

Genomic DNA of *A. oryzae* was prepared using a previously described method [17]. The G6PDH coding gene *gsd* was amplified from *A. oryzae* genomic DNA using the primers P1/P2 designed from the putative *gsd* from *A. oryzae* RIB40 (Dogan AO 090005001427) (Table S1). PCR product was purified and cloned into pUC19T vector to obtain the cloning plasmid pUC19-*gsd*-DNA, which was followed by sequencing conducted by Invitrogen (China).

Bioinformatic Analysis

The *gsd* and corresponding cDNA sequences were deduced with the putative G6PDH from *A. oryzae* RIB40 (NCBI reference sequence: XP_001818354.2) as a reference sequence using the DNAMAN program. The protein modelling was constructed using SWISS-MODEL [18] and multiple sequence alignment was performed using CLUSTALW 2.1.

Heterogeneous Expression and Purification of G6PDH

To eliminate the effects of intron from *A. oryzae* CICC2012 on heterogeneous expression in the cells of *E. coli*, the cDNA of *A. oryzae* CICC2012 was reverse transcribed and synthesized from general RNA of the fungi cell. The synthesized cDNA was used as PCR template subsequently. PCR gene specific primers for *A. oryzae* CICC2012 *gsd* were designed from the putative G6PDH from *A. oryzae* RIB40 (NCBI reference sequence: XP_001818354.2). The putative *gsd* was amplified by two-step fusion PCR, using three pairs of oligonucleotide primers (Table S1). Primers 1F/1R and 2F/2R were used to amplify *gsd*-F1 and *gsd*-F2 respectively, and primers 3F/3R were utilized to fuse the *gsd*-F1 and *gsd*-F2 to the complete sequence. The fusion PCR product was purified, and subsequently cloned into pUC19 vector (Sangon, China) to construct the recombined plasmid pUC19-*gsd*-cDNA, which was followed by sequencing. pUC19-*gsd*-cDNA was extracted by Spin Column Plasmid Mini-Preps Kit (Sangon), and was digested by

Bam HI and *Not* I. The digestion production was cloned into the pET-28a(+) vector (Novagen, USA) to generate the recombinant plasmid pET-*gsd*-cDNA.

The recombinant plasmid pET-*gsd*-cDNA was transformed into cells of *E. coli* BL21 (DE3) and transformants were selected from LB medium containing 100 μg/ml ampicillin, which resulted in recombinant strain *E. coli* BL21-*gsd*. The fresh colony of *E. coli* BL21-*gsd* grown in LB media was transferred into TB medium with 100 μg/ml ampicillin at 37°C for 2–3 h. When cell density OD_{600} reached 0.6–0.8, protein was induced by addition of 1 mM IPTG at 25°C for 12 h. To protect the soluble protein, 2 mM DL-Dithiothreitol was added into 1 ml suspension culture [19]. Cells were harvested and sonicated on ice which was followed by centrifugation at 12,000 ×*g* for 15 min at 4°C. The supernatant was loaded onto a Ni^{2+}-chelated (5 ml) column (CW Bio, China), which was pre-equilibrated with buffer A (0.5 M NaCl and 10 mM imidazole). Elution was performed with buffer B (0.5 M NaCl and 500 mM imidazole). The elution product was gel-filtrated with a Superdex 200 column (1 × 30 cm), which was pre-equilibrated and eluted with buffer C (0.5 M NaCl). SDS-PAGE was performed using 12% separating gel to assess the purity and molecular weight of the recombinant G6PDH. Protein concentrations were determined using Bradford's assay with bovine serum albumin as the protein standard [20].

Enzyme Activity Assays

The activity of G6PDH was determined using the methods described with modifications [21]. G6PDH activities were measured by monitoring NADPH formation at 340 nm and at 25°C on a spectrophotometer, equipped with a thermo-stated cuvette holder. 200 μl of the standard assay solution containing 50 mM Tris-HCl buffer (pH 7.5), 5 mM $MgCl_2$, 0.4 mM $NADP^+$ and 10 mM G6P was utilized. The reaction was initiated by adding an appropriate amount of enzyme and the initial velocity of the reaction were assayed for 60 s. One unit of G6PDH activity is the amount of enzyme catalyzing the formation of 1 μmol of NADPH per minute under the assay conditions. Specific enzyme activity (U/mg) is defined as units per mg of protein.

Biochemical Characterization

The optimal pH was determined at 25°C using 100 mM Na_2HPO_4-citric acid buffer (pH 5.0–6.0), 100 mM Na_2HPO_4-NaH_2PO_4 buffer (pH 6.5–7.5) and 100 mM Tris-HCl buffer for pH 8.0–9.0, respectively. Optimal temperature was measured from 20 to 60°C in 100 mM Na_2HPO_4-NaH_2PO_4 buffer (pH 7.5). To investigate thermo stability, the G6PDH was incubated at 40°C, 45°C, 50°C, and 55°C at different time intervals in 100 mM Na_2HPO_4-NaH_2PO_4 buffer (pH 7.5). The residual activity was assayed to determine the half-lives of G6PDH. To analyze the effects of various metal ions on the activity of G6PDH, 1 mM (final concentrations) of Fe^{2+}, Zn^{2+}, Cu^{2+}, Mg^{2+}, Ba^{2+}, Ca^{2+}, K^+, and Mn^{2+} were added individually during the enzymatic activity assessment.

Kinetics Study

Substrate kinetics were determined at 25°C in 1 ml reaction mixtures containing 50 mM Tris–HCl buffer (pH 7.5), 5 mM $MgCl_2$ and various concentrations of G6P and $NADP^+$. A matrix of substrate and coenzyme combinations between 100~500 μM G6P and 10~100 μM $NADP^+$ was performed and the reactions were initiated by the addition of enzyme. Catalytic inhibition of G6PDH by NADPH was performed by varying the concentrations of NADPH utilized in the reaction mixture. To assay the inhibition profile of NADPH, one substrate with saturating concentrations (10 mM G6P or 0.40 mM $NADP^+$) and the other with unsaturated content were utilized in the mixture. The kinetic parameters were calculated by curve-fitting to the steady-state sequential kinetic equation 1:

$$V = \frac{V_{max}[A][B]}{K_B[A]+K_A[B]+K_{iA}K_B+[A][B]} \quad (1)$$

Wherein A and B represent substrates $NADP^+$ and G6P, respectively. V_{max} is the maximum velocity and K_{iA} is the dissociation constant of substrate A from the binary complex EA. K_A and K_B are the Michaelis constant K_m for substrates A and B, respectively [22]. K_m and V_{max} were drawn from a two-round double reciprocal plot using Origin Pro 8.0 software (Origin Lab Corporation).

Results

Cloning and Sequence Analysis of G6PDH in *A. oryzae* CICC2012

As the genome sequence of *A. oryzae* CICC2012 has not been reported, the ORF of *gsd* from this fungus was deduced by utilizing the hypothesized G6PDH from *A. oryzae* RIB40. According to the putative G6PDH from *A. oryzae* RIB40 (Dogan AO 090005001427), primers P1/P2 were designed. The expected 2.8 kb *gsd* was amplified from *A. oryzae* CICC2012 genomic DNA using the primers P1/P2, and then cloned into pUC19T vector obtaining the plasmid pUC19-*gsd*-DNA. To eliminate intron, general RNA was extracted from *A. oryzae* CICC2012 mycelia and reversed transcribed into cDNA using a reverse transcriptase to synthesize cDNA. The synthesized cDNA was used as PCR template for the amplification of the *gsd*. As illustrated in Fig. S1, a putative *gsd* with an expected size of 1.5 kb was obtained by a two-step fusion PCR reaction from cDNA, which was followed by cloning into pET-28a (+) to generate the expression plasmid pET-*gsd*-cDNA.

DNA sequencing of pUC19-*gsd*-DNA and pET-*gsd*-cDNA showed that the ORF and coding sequence (CDS) of *gsd* of *A. oryzae* CICC2012 were totally identical to their counterparts from *A. oryzae* RIB40 hypothesized *gsd* respectively. The

obtained cDNA of *A. oryzae* CICC2012 G6PDH was deposited in Genbank with accession number JN123468. The *gsd* ORF obtained from *A. oryzae* CICC2012 was 2,837 bp including five introns. The six introns of *gsd* were located at 1,033–1,199 bp, 1,305–1,357 bp, 1,442–1,500 bp, 1,581–1,634 bp, 1,841–1,893 bp, respectively. Meanwhile, the CDS was 1,533 bp encoding 510 amino acids with an estimated molecular weight of 58.8 kDa.

Multiple sequence alignment of the deduced amino acid sequence of G6PDH showed high similarity to its homologies from *Aspergillus flavus* (99%) and *Aspergillus niger* (97%), but less to *S. cerevisiae* (59%). The similarity of different G6PDHs was consistent with the phylogenetic distance of different organisms (data not shown). A motif (RXXXEKPXG) in the coenzyme-binding site and three conserved motifs (annotation) (RIDHYLGK, EXXGXEXRXXY and DXXQNH) in the substrate-binding site were also observed in AoG6PDH (Fig. S2), indicating the G6P and $NADP^+$ binding and catalyzing residues were highly conserved [21]. The secondary structure of the protein was analyzed, the α-helix region occupied 46.7%, the β-sheet was 12.8% and the random coil was 40.6% (Fig. S3).

Heterogenous Expression and Purification of AoG6PDH

The recombinant strain *E. coli* BL21-*gsd* was obtained by transformation of expression plasmid pET-*gsd*-cDNA. Cellular lysate of *E. coli* BL21-*gsd* was subjected to SDS-PAGE analysis (Fig. 2A), an over-expressed band with a size of around 55.0 kDa was observed, in accordance with the expected value 58.8 kDa. A leaky expression profile was also observed as the target protein band was obtained without IPTG. A 12.9 U/(mg·protein) specific activity of

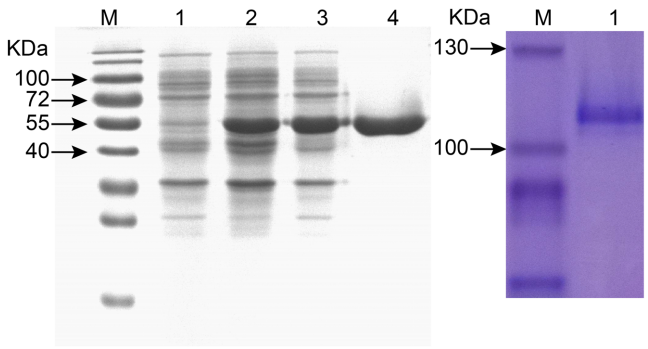

Fig. 2. Purification of heterogeneous expression of AoG6PDH. A: SDS-PAGE, Lane M: protein molecular mass marker; Lane 1: the lysate of *E. coli* BL21 (DE3); Lane 2: the lysate of *E. coli* BL21-*gsd* incubated without IPTG; Lane 3: the lysate of *E. coli* BL21-*gsd* incubated with IPTG; Lane 4: the purified AoG6PDH. B: Native-PAGE, Lane M: protein molecular mass marker; Lane 1: the purified AoG6PDH.

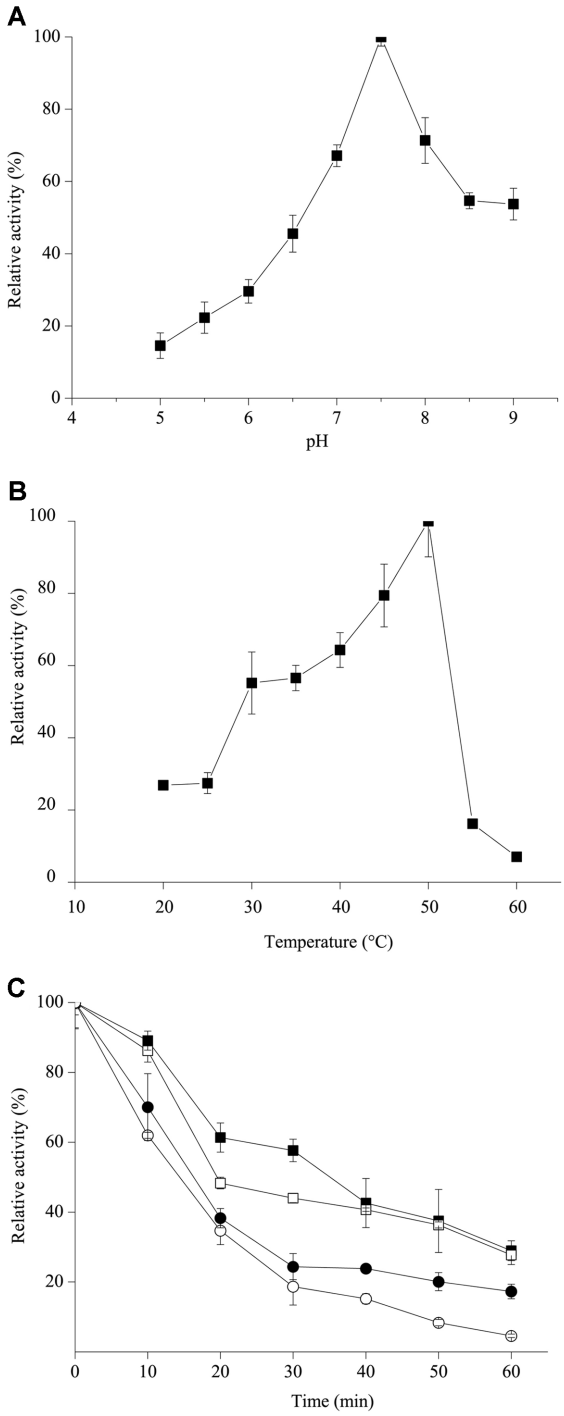

Fig. 3. The effects of pH (**A**) and temperature (**B**) on activity of recombinant AoG6PDH. The thermostability analysis of recombinant AoG6PDH (**C**), ■: 40°C, □: 45°C, ●: 50°C, ○: 55°C.

G6PDH was detected in the cellular lysate and then the recombinant G6PDH was purified to electrophoretic homogeneity by affinity chromatography (Fig. 2A). The specific activity of purified G6PDH was 73.6 U/(mg·protein) with a recovery yield of 56.3% and 6.1-fold purification. No enzyme activity was detected when NAD^+ was used as the coenzyme, as the purified G6PDH exhibited strictly $NADP^+$-dependent specificity. The $NADP^+$-dependent G6PDH of the purified product had high activity, which proved that the putative sequence was the encoding sequence of G6PDH.

Based on observation with Native-PAGE, AoG6PDH was a homodimer with an estimated molecular weight of 118.0 kDa (Fig. 2B). The observation suggested that G6PDH was a homodimer, which was similar to G6PD from *L. mesenteroides* (dimer, LmG6PDH) [23] but different from sheep brain cortex G6PD (monomer) [24], *Brugia malayi* G6PD (tetramer) [25], human erythrocytes G6PD (switch between dimer and tetramer) [26] and rat liver G6PD (regularly forms hexamers) [16]. The protein modelling of AoG6PDH shown in Fig. S4 was constructed using SWISS-MODEL, which coincided with the observation using Native-PAGE.

Biochemical Characterization of AoG6PDH

The effects of pH and temperature on G6PDH activity were examined in the presence of G6P and $NADP^+$, respectively. The optimal pH of G6PDH was around 7.5 (Fig. 3A). About 70% of G6PDH activities remained at pH 7.0 and 8.0. The enzyme had a similar pH profile to that of the other G6PDHs (Table 2). The optimal temperature was around 50°C (Fig. 3B), which was similar to the known

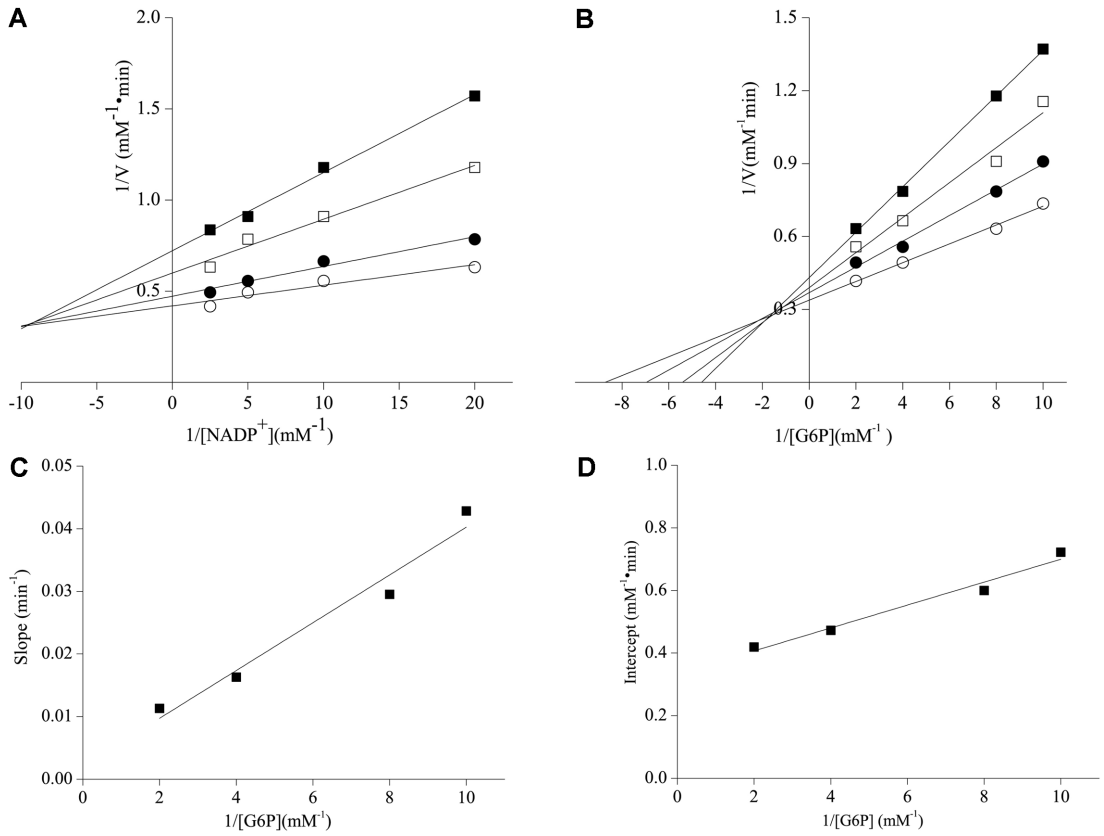

Fig. 4. Initial velocity analyses for $NADP^+$-dependent AoG6PDH.

A: Primary double reciprocal plot of 1/V versus 1/[$NADP^+$] at several fixed concentrations of G6P, 0.100 mM G6P (■), 0.125 mM G6P (□), 0.250 mM G6P (●), 0.500 mM G6P (○), and the corresponding R^2 value of each plot was 0.99, 0.96, 0.95 and 0.90 respectively. B: Primary double reciprocal plot of 1/V versus 1/[G6P] at several fixed concentrations of $NADP^+$, 0.050 mM $NADP^+$ (■), 0.100 mM $NADP^+$ (□), 0.200 mM $NADP^+$ (●), 0.400 mM $NADP^+$ (○), and the corresponding R^2 value of each plot was 0.99, 0.95, 0.98 and 0.99 respectively. C: Secondary plot of slopes of lines from primary plot A versus 1/[G6P], and the R^2 was 0.95. D: Secondary plot of intercepts of lines from primary plot A versus 1/[G6P], and the R^2 value was 0.96. The data represent the averages of duplicate runs.

G6PDHs (30–92°C) [21]. The G6PDH had an approximately 60–80% of its maximum activity at 35–45°C, but only ~2 and ~30% of its maximum activity at 60°C and 20°C were gauged, respectively.

The thermostability of G6PDH was observed and showed that about 60% of activity was maintained under a condition of 40°C after incubation for 30 min with a half-life following first-order kinetics of 33.3 min (Fig. 3C). However, when the temperature was above 50°C, the activity of G6PDH decreased rapidly and the half-life of was only 16.3 min and 13.6 min at 50°C and 55°C, respectively.

The effects of different metal ions on G6PDH activity were also investigated. Compared to the control reaction without metal ions, Zn^{2+}, Cu^{2+}, Mg^{2+} notably enhanced its activity (273%, 237%, and 192%, respectively). Ca^{2+} and Fe^{3+} had no obvious effect (109% and 98%). K^{+} and Mn^{2+} presented an inhibition effect (84% and 28%).

Kinetic Properties of Recombinant AoG6PDH

To elucidate the kinetic mechanism, the recombinant AoG6PDH was used for two substrate, steady-state kinetic analysis. Initial velocity experiments provided clues to differentiate sequential from ping-pong mechanism. The initial velocity studies were performed by measuring G6PDH activity varying the concentrations of G6P and $NADP^{+}$ at several fixed concentrations. The results were represented on Lineweaver-Burk plots. The corresponding set of the double reciprocal plots were linear and converged to the left of the Y-axis with R^2 values of 0.90 to 0.99 respectively (Figs. 4A and 4B). Accordingly, the ping-pong mechanism was excluded and the kinetic mechanism of the enzyme was deemed to be sequential. To determine whether it was a steady-state ordered or a rapid equilibrium random BiBi mechanism, the secondary plots of these slopes and intercepts versus the reciprocal of fixed substrate concentrations were implemented. A set of straight lines was obtained with values of 0.96 and 0.99 respectively (Figs. 4C and 4D), which supported a sequential mechanism for the AoG6PDH.

Product inhibition studies were performed to ascertain the substrate binding profile and product releasing profile. Because of the instability of the 6-phosphoglucono-δ-lactone (6PGDL), only NADPH inhibition experiments were performed. The double reciprocal plots of initial velocity versus several fixed concentrations of NADPH yielded a series of lines intersecting with R^2 values of 0.96 to 0.99 respectively. These results indicated that NADPH exhibited a competitive inhibition with respect to $NADP^{+}$ (Fig. 5A) and a linear mixed inhibition with respect to G6P (Fig. 5B). The inhibition pattern coincided with the steady-state ordered BiBi mechanism, where $NADP^{+}$ is the first substrate bound to the enzyme and NADPH is the second product released from the enzyme.

A general description of two substrate ordered reactions was given by Eq. (1), where A and B represented the first bonding substrate $NADP^{+}$ and the second G6P, respectively. Secondary plots of intercepts and slopes of lines from the

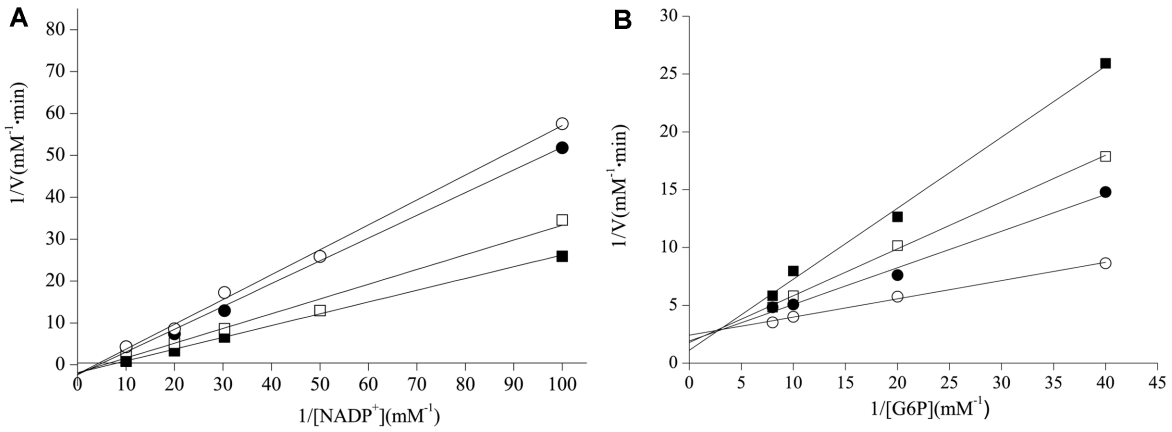

Fig. 5. Double-reciprocal plot of inhibition of G6PDH by several fixed concentrations of NADPH, with respect to $NADP^{+}$ (**A**) and G6P (**B**).

■: 0.000 mM NADPH, □: 0.025 mM NADPH, ●: 0.050 mM NADPH, ○: 0.075 mM NADPH respectively. The corresponding R^2 value of each plot in A was 0.99 (■), 0.97 (□), 0.99 (●) and 0.99 (○), respectively. R^2 value of each plot in B was 0.99 (■), 0.99 (□), 0.98 (●) and 0.99 (○) respectively. The data represent the averages of duplicate runs.

Table 1. Kinetic parameters of G6PDH from *A. oryzae*.

Substrate	K_m (μM)	K_i (μM)	V_{max} (u·ml^{-1})	k_{cat} (s^{-1})	k_{cat}/K_m (s^{-1}·μM^{-1})
G6P	109.7	-	3.0	1000.0	9.1
$NADP^+$	6.3	16.7	3.0	1000.0	158.7

-: not detected

main plot with 1/ [G6P] as the variable can be utilized to estimate the kinetic constants (Fig. 4B). The obtained kinetic constants were listed in Table 1.

Discussion

Regulation of intracellular cofactor content and its regeneration is both of academic and application relevance for desired metabolite production in cellulolytic fungi using CBP technologies. To characterize the rate-limiting catalytic step in the PP pathway by G6PDH in *A. oryzae* CICC2012, which was one of the best potential targets for enhancing cofactor generation, the enzyme was heterogeneously expressed and functionally characterized.

According to the specificity of coenzyme, G6PDH can be divided into three categories: $NADP^+$-strictly specific, $NADP^+$-preferred and NAD^+-preferred dual coenzyme specificity. Most G6PDH reported are strictly $NADP^+$-dependent or $NADP^+$-preferred enzymes, a few can also utilize NAD^+. The recombinant AoG6PDH did not show any activity when NAD^+ was used as the coenzyme, exhibiting strictly $NADP^+$-dependent specificity. G6PDHs from other *Aspergillus* species, such as *A. niger* [27], *A. nidulans* [27], *A. parasiticus* [28] and *A. aculeatus* [29], also exhibited strict specificity towards $NADP^+$. In all $NADP^+$-preferred G6PDHs, the conserved Arg residue was revealed and identified as a determinant in the $NADP^+$ specificity [21]. The conserved Arg residue binds tightly with the negatively charged phosphate group of $NADP^+$ via forming an electrostatic interaction [21]. The corresponding Arg residue was assessed in AoG6PDH, while, in some dual coenzyme specific enzymes the corresponding Arg residue still existed [30]. According to the crystallographic structure of dual coenzyme specific LmG6PDH, the dual coenzyme specificity was also associated with key residues surrounding conserved Arg residue and oligomeric states switching between binary and ternary enzyme complexes [15, 23].

Two substrate, steady-state kinetic analyses were used for elucidating the kinetic mechanism of the $NADP^+$-dependent AoG6PDH. The double reciprocal plots of the initial velocity have a linear intersecting pattern, which excludes the ping-pong mechanism. Since NADPH is a competitive inhibitor to $NADP^+$ and a mixed inhibitor to G6P, an ordered BiBi mechanism fits our data best, in which $NADP^+$ is the first substrate bound to the enzyme, and NADPH is the second product dissociated from the enzyme complex.

A similar mechanism has been proposed for G6PDHs

Table 2. Properties of G6PDH from various organisms.

Organism	Subunit mol mass (kDa)	Native mol mass (kDa)	k_{cat} (s^{-1})	K_m for G6P (μM)	k_{cat}/K_m for G6P (s^{-1}·μM^{-1})	K_m for $NADP^+$ (μM)	k_{cat}/K_m for $NADP^+$ (s^{-1}·μM^{-1})	Optimal pH
A. oryzae (this work)	58.8	118	1000	109.7	9.1	6.3	158.7	7.5
A. niger[27]	57-60	160	ND	153	ND*	26	ND	9.0
A. nidulms [27]	53-55	180	ND	92	ND*	30	ND	9.0
A. aculeatus [29]	52	105	83	75	1.1	6	14	7.5
Y. lipolytica [21]	55	219	182.7	264.9	0.58	33.3	5.49	8.5
T. maritima [38]	60	95	35000	200	175	40	890	7.4
P. aeruginosa [39]	55.6	250 or 500	540	498.7	2.38	56.7	9.52	8.8
E. coli DH5*a* [41]	55	117	32.5	224	0.15	127	0.26	8.0
T. cruzi [42]	62	158	62	77	0.8	16	3.2	7.5
T. crassiceps [43]	61	134	34	14	2.43	1.3	26.1	7.8
Human [40]	57	220	275	52	5.31	7.07	39.7	8.0

*ND: not detected

from human, pig and rat liver [31], human placental [32], human erythrocyte [26], bovine lens [33], *Corynebacterium glutamicum* [34], and *Schizosaccharomyces pombe* [35]. For G6PDH from lamb kidney cortex, an ordered mechanism has been deduced from inhibition studies, but with G6P as the first substrate bound to the enzyme [24]. In the kinetic mechanism studies of G6PDHs from some other sources such as fungi and mammals, rabbit erythrocytes, rat breast, and bovine adrenals, it was shown that the enzymes follow a random BiBi mechanism [27]. The enzyme purified from *L. mesenterroides* can use both NAD^+ and $NADP^+$ as substrates. When NAD^+ was the substrate, the enzyme obeys a random BiBi, otherwise it obeys an ordered BiBi mechanism [36]. The kinetic studies on recombinant human G6PD suggested that the enzyme follows either random or ordered mechanisms [37].

The K_m values of AoG6PDH were calculated as 109.7 and 6.3 mM for G6P and $NADP^+$, respectively. The K_m value for $NADP^+$ was lower than that for G6P, suggesting the higher affinity of AoG6PDH to $NADP^+$ when compared with G6P, similar to those in other studies (Table 2). The catalytic efficiency (k_{cat}/K_m) for G6P and $NADP^+$ was 9.1 and 158.7 $s^{-1}\cdot\mu M^{-1}$, respectively, suggesting that the enzyme was more efficient with $NADP^+$ as the substrate. Table 2 displays the kinetic characteristics of purified G6PDHs from various organisms. Compared to these enzymes, except *T. maritime* G6PDH [38], AoG6PDH has both higher k_{cat} and catalytic efficiencies (k_{cat}/K_m) with respect to G6P and $NADP^+$. Its k_{cat} is 11-fold higher than the *Aspergillus* enzyme (*A. aculeatus* G6PDH) [29] and 85% higher than *P. aeruginosa* G6PDH [39]. Its catalytic efficiency with respect to $NADP^+$ was 7-fold higher than that of the human G6PDH [40] and 5-fold higher than that of any of the other G6PDHs.

In conclusion, putative G6PDH from industrial *A. oryzae* CICC2012 has now been identified and characterized by heterogeneous expression and purification for the first time. The recombined protein exhibited strictly $NADP^+$-dependent activity, which discriminated the complex catalytic mechanism. The established kinetic model could be applied in further regulation of the pentose phosphate pathway and intracellular content of NADPH/$NADP^+$ for improving the xylose utilization and yields of valued metabolites.

Acknowledgments

This work was supported by grants from the National Natural Science Foundation of China (No. 21476093 and 21706084), the Natural Science Foundation of Fujian Province (No. 2018J01010) and the Scientific Research Funds of Huaqiao University (16BS103).

Conflict of Interest

The authors have no financial conflicts of interest to declare.

References

1. Olson DG, McBride JE, Shaw AJ, Lynd LR. 2012. Recent progress in consolidated bioprocessing. *Curr. Opin. Biotechnol.* **23:** 396-405.
2. Bourdichon F, Casaregola S, Farrokh C, Frisvad JC, Gerds ML, Hammes WP, *et al.* 2012. Food fermentations: microorganisms with technological beneficial use. *Int. J. Food Microbiol.* **154:** 87-97.
3. Szabo OE, Csiszar E, Koczka B, Kiss K. 2015. Ultrasonically assisted single stage and multiple extraction of enzymes produced by *Aspergillus oryzae* on a lignocellulosic substrate with solid-state fermentation. *Biomass Bioenergy* **75:** 161-169.
4. Lin H, Wang Q, Shen Q, Ma J, Fu J, Zhao Y. 2014. Engineering *Aspergillus oryzae* A-4 through the chromosomal insertion of foreign cellulase expression cassette to improve conversion of cellulosic biomass into lipids. *PLoS One* **9:** e108442.
5. El-Ghonemy DH, Ali TH, El-Bondkly AM, Moharam Mel S, Talkhan FN. 2014. Improvement of *Aspergillus oryzae* NRRL 3484 by mutagenesis and optimization of culture conditions in solid-state fermentation for the hyper-production of extracellular cellulase. *Antonie Van Leeuwenhoek* **106:** 853-864.
6. Hirayama K, Watanabe H, Tokuda G, Kitamoto K, Arioka M. 2010. Purification and characterization of termite endogenous beta-1,4-endoglucanases produced in *Aspergillus oryzae*. *Biosci. Biotechnol. Biochem.* **74:** 1680-1686.
7. Maas RH, Springer J, Eggink G, Weusthuis RA. 2008. Xylose metabolism in the fungus *Rhizopus oryzae*: effect of growth and respiration on L(+)-lactic acid production. *J. Ind. Microbiol. Biotechnol.* **35:** 569-578.
8. Xu Q, Li S, Fu Y, Tai C, Huang H. 2010. Two-stage utilization of corn straw by *Rhizopus oryzae* for fumaric acid production. *Bioresour. Technol.* **101:** 6262-6264.
9. Tran LH, Kitamoto N, Kawai K, Takamizawa K, Suzuki T. 2004. Cloning and expression of a NAD^+-dependent xylitol dehydrogenase gene (*xdhA*) of *Aspergillus oryzae*. *J. Biosci. Bioeng.* **97:** 419-422.
10. Runquist D, Hahn-Hagerdal B, Bettiga M. 2010. Increased ethanol productivity in xylose-utilizing *Saccharomyces cerevisiae* via a randomly mutagenized xylose reductase. *Appl. Environ. Microbiol.* **76:** 7796-7802.

11. Chin JW, Cirino PC. 2011. Improved NADPH supply for xylitol production by engineered *Escherichia coli* with glycolytic mutations. *Biotechnol. Prog.* **27:** 333-341.
12. Ahmad I, Shim WY, Kim JH. 2013. Enhancement of xylitol production in glycerol kinase disrupted *Candida tropicalis* by co-expression of three genes involved in glycerol metabolic pathway. *Bioprocess Biosyst. Eng.* **36:** 1279-1284.
13. Oh EJ, Ha SJ, Rin Kim S, Lee WH, Galazka JM, Cate JH, *et al.* 2013. Enhanced xylitol production through simultaneous co-utilization of cellobiose and xylose by engineered *Saccharomyces cerevisiae*. *Metab. Eng.* **15:** 226-234.
14. Au SW, Gover S, Lam VM, Adams MJ. 2000. Human glucose-6-phosphate dehydrogenase: the crystal structure reveals a structural $NADP^+$ molecule and provides insights into enzyme deficiency. *Structure* **8:** 293-303.
15. Ranzani AT, Cordeiro AT. 2017. Mutations in the tetramer interface of human glucose-6-phosphate dehydrogenase reveals kinetic differences between oligomeric states. *FEBS Lett.* **591:** 1278-1284.
16. Temel Y, Kocyigit UM. 2017. Purification of glucose-6-phosphate dehydrogenase from rat (*Rattus norvegicus*) erythrocytes and inhibition effects of some metal ions on enzyme activity. *J. Biochem. Mol. Toxicol.* **31(9)**.
17. Du Y, Xie G, Yang C, Fang B, Chen H. 2014. Construction of brewing-wine *Aspergillus oryzae* $pyrG^-$ mutant by *pyrG* gene deletion and its application in homology transformation. *Acta. Biochim. Biophys. Sin. (Shanghai)* **46:** 477-483.
18. Waterhouse A, Bertoni M, Bienert S, Studer G, Tauriello G, Gumienny R, *et al.* 2018. SWISS-MODEL: homology modelling of protein structures and complexes. *Nucleic Acids Res.* **46:** W296-W303.
19. Bradford MM. 2015. A rapid method for quantitation of microgram quantities of protein utilizing the principle of protein-dye binding. *Anal. Biochem.* **72:** 248–254.
20. Kruger NJ. 2002. The Bradford method for protein quantitation, pp. 15-21. *The protein protocols handbook*, Springer,
21. Bian M, Li S, Wei H, Huang S, Zhou F, Zhu Y, *et al.* 2018. Heteroexpression and biochemical characterization of a glucose-6-phosphate dehydrogenase from oleaginous yeast *Yarrowia lipolytica*. *Protein Expr. Purif.* **148:** 1-8.
22. Purich DL. 2010. *Enzyme kinetics: catalysis and control: a reference of theory and best-practice methods*, pp. 335-338. 1st Ed. Elsevier.
23. Naylor CE, Gover S, Basak AK, Cosgrove MS, Levy HR, Adams MJ. 2001. $NADP^+$ and NAD^+ binding to the dual coenzyme specific enzyme *Leuconostoc mesenteroides* glucose 6-phosphate dehydrogenase: different interdomain hinge angles are seen in different binary and ternary complexes. *Acta crystallogr. D. Biol. Crystallogr.* **57:** 635-648.
24. Ulusu NN, Tandogan B, Tezcan FE. 2005. Kinetic properties of glucose-6-phosphate dehydrogenase from lamb kidney cortex. *Biochimie* **87:** 187-190.
25. Verma A, Suthar MK, Doharey PK, Gupta S, Yadav S, Chauhan PMS, *et al.* 2013. Molecular cloning and characterization of glucose-6-phosphate dehydrogenase from *Brugia malayi*. *Parasitology* **140:** 897-906.
26. Adediran SA. 1991. Kinetic properties of normal human erythrocyte glucose-6-phosphate dehydrogenase dimers. *Biochimie.* **73:** 1211-1218.
27. Wennekes LM, Goosen T, van den Broek PJ, van den Broek HW. 1993. Purification and characterization of glucose-6-phosphate dehydrogenase from *Aspergillus niger* and *Aspergillus nidulans*. *J. Gen. Microbiol.* **139:** 2793-2800.
28. Jr NW, Jr DR. 1984. Purification and characterization of glucose-6-phosphate dehydrogenase from *Aspergillus parasiticus*. *Arch. Biochem. Biophys.* **228:** 113-119.
29. Omodele Ibraheem IOAaAA. 2005. Purification and properties of glucose 6-phosphate dehydrogenase from *Aspergillus aculeatus*. *J. Biochem. Mol. Biol.* **38:** 584-590.
30. Rowland P, Basak AK, Gover S, Levy HR, Adams MJ. 1994. The three–dimensional structure of glucose 6–phosphate dehydrogenase from *Leuconostoc mesenteroides* refined at 2.0 Å resolution. *Structure* **2:** 1073-1087.
31. Shreve DS, Levy HR. 1980. Kinetic mechanism of glucose-6-phosphate dehydrogenase from the lactating rat mammary gland. Implications for regulation. *J. Biol. Chem.* **255:** 2670-2677.
32. Aksoy Y, Ogüs IH, Oauzer N. 2001. Purification and some properties of human placental glucose-6-phosphate dehydrogenase. *Protein Expr. Purif.* **21:** 286-292.
33. Ulusu NN, Kus MS, Acan NL, Tezcan EF. 1999. A rapid method for the purification of glucose-6-phosphate dehydrogenase from bovine lens. *Int. J. Biochem. Cell Biol.* **31:** 787-796.
34. Moritz B, Striegel K, Graaf AA, De, Sahm H. 2010. Kinetic properties of the glucose-6-phosphate and 6-phosphogluconate dehydrogenases from *Corynebacterium glutamicum* and their application for predicting pentose phosphate pathway flux in vivo. *FEBS J.* **267:** 3442-3452.
35. Tsai CS, Chen Q. 1998. Purification and kinetic characterization of hexokinase and glucose-6-phosphate dehydrogenase from *Schizosaccharomyces pombe*. *Biochem. Cell Biol.* **76:** 107-113.
36. Levy HR, Christoff M, Ingulli J, Ho EML. 1983. Glucose-6-phosphate dehydrogenase from *Leuconostoc mesenteroides*: Revised kinetic mechanism and kinetics of ATP inhibition. *Arch. Biochem. Biophys.* **222:** 473-488.
37. Wang XT, Au SW, Lam VM, Engel PC. 2002. Recombinant human glucose-6-phosphate dehydrogenase. Evidence for a rapid-equilibrium random-order mechanism. *Eur. J. Biochem.* **269:** 3417-3424.
38. Hansen T, Schlichting B, Schonheit P. 2002. Glucose-6-phosphate dehydrogenase from the hyperthermophilic bacterium *Thermotoga maritima*: expression of the g6pd gene and characterization of an extremely thermophilic enzyme. *FEMS Microbiol. Lett.* **216:** 249-253.

39. Acero-Navarro KE, Jimenez-Ramirez M, Villalobos MA, Vargas-Martinez R, Perales-Vela HV, Velasco-Garcia R. 2018. Cloning, overexpression, and purification of glucose-6-phosphate dehydrogenase of *Pseudomonas aeruginosa*. *Protein Expr. Purif.* **142:** 53-61.
40. Wang XT, Lam VM, Engel PC. 2005. Marked decrease in specific activity contributes to disease phenotype in two human glucose 6-phosphate dehydrogenase mutants, G6PD(Union) and G6PD(Andalus). *Hum. Mutat.* **26:** 284.
41. Schuurmann J, Quehl P, Lindhorst F, Lang K, Jose J. 2017. Autodisplay of glucose-6-phosphate dehydrogenase for redox cofactor regeneration at the cell surface. *Biotechnol. Bioeng.* **114:** 1658-1669.
42. Ortiz C, Moraca F, Medeiros A, Botta M, Hamilton N, Comini MA. 2016. Binding mode and selectivity of steroids towards glucose-6-phosphate dehydrogenase from the pathogen *Trypanosoma cruzi*. *Molecules* **21:** 368.
43. Rendón JL, del Arenal IP, Guevara-Flores A, Mendoza-Hernández G, Pardo JP. 2008. Glucose 6-phosphate dehydrogenase from larval *Taenia crassiceps* (cysticerci): purification and properties. *Parasitol. Res.* **102:** 1351-1357.